



## Predicting micro-catchment infiltration dynamics

Michael J. Founds<sup>a,\*</sup>, Kenneth C. McGwire<sup>a</sup>, Mark A. Weltz<sup>b</sup>, Sayjro K. Nouwakpo<sup>c</sup>,  
Paul S.J. Verburg<sup>d</sup>

<sup>a</sup> Desert Research Institute, Reno, Nevada, USA

<sup>b</sup> U.S. Dept. of Agriculture Agricultural Research Service, Reno, Nevada, USA

<sup>c</sup> U.S. Dept. of Agriculture Agricultural Research Service, Kimberly, ID, USA

<sup>d</sup> University of Nevada, Reno, Nevada, USA

### ABSTRACT

Rainfall and concentrated flow experiments were carried out on seven micro-catchments (MCs) that were designed to limit soil erosion and allow for water harvesting. Prediction of infiltration rates within MCs is necessary to design effective hillslope-scale restoration projects. Continuous stage measurements and 3-D models of MC geometry were used to calculate infiltration rates from field experiments. Soil samples and Guelph permeameter (GP) measurements were collected to parameterize a predictive infiltration model in Hydrus 2D/3D. The model result of water velocity into the soil profile was averaged by depth intervals and multiplied by the corresponding MC surface area to calculate a volumetric flow rate. Four parameterizations of changes in conductivity with depth were evaluated within the model framework to determine which would best account for spatial heterogeneity. Use of the maximum field-measured conductivity provided the least biased results, with average error between simulated and measured values across all sites of less than 1%. Model results illustrate the limitations associated with particle-size distribution or GP measurements when used to predict infiltration rates in a numerical model. GP measurements with single ponded heights allowed convenient field measurement of conductivity that worked better than predictions from soil texture. The maximum of several GP samples was more representative of MC infiltration than the mean, so a higher percentile value from a distribution of MC measurements may help to account for complex infiltration processes that are not included in numerical models. This modeling approach will allow testing of process-based hypotheses about rangeland infiltration dynamics, and the development of optimal configurations of MCs at sites being considered for rangeland restoration.

### 1. Introduction

#### 1.1. Micro-catchment water harvesting

Micro-catchments (MCs) traditionally have been used for water harvesting in arid areas where runoff is captured within pits to increase its availability for plant growth (Alshawahneh et al., 2011; Malagnoux, 2008; Oweis, 2016; Previati et al., 2010; Schiettecatte et al., 2005). The MCs capture storm runoff, thus dissipating the erosive energy of flowing water and allowing the water to infiltrate into the soil. The Vallerani® System was originally developed in 1988 to mechanize rainwater harvesting techniques with special plows that create crescent-shaped pits (Gammoh and Oweis, 2011; Oweis et al., 2011). The Vallerani System has been applied to nearly 100,000 ha of degraded rangeland in Morocco, Niger, Senegal, Sudan, Tunisia, Chad and Egypt (Malagnoux, 2008). The Badia Benchmark Study (Oweis et al., 2011) carried out in Jordan and Syria found that intermittent contours created by the Vallerani plow proved to be an economical way to establish vegetation and reduce soil erosion; 20 ha of MCs could be constructed per day at a cost of \$32 USD/ha (Oweis, 2016). Despite wide application of this restoration strategy, our understanding of the infiltration dynamics of

MCs during large rainfall events is limited. A method to predict MC infiltration during large rainfall events is necessary to design successful rangeland restoration projects.

#### 1.2. Physically based infiltration models

An accurate representation of how MCs function during large runoff events requires consideration of ponded infiltration into a complex soil profile. For unsaturated flow, where the soil water content ( $\theta$ ) is less than the saturated water content ( $\theta_s$ ), the unsaturated hydraulic conductivity  $K(\psi)$  is related to a function of capillary pressure head ( $\psi$ ). The matric potential ( $\psi$ ) refers to areas of negative pressure observed in the variably saturated zone and can be alternatively expressed as negative potential ( $-h$ ). A positive  $h$  value can be referred to as hydrostatic potential, while a negative  $h$  value could be called matric potential.

By combining the work of Darcy (1856) and Buckingham (1907) with the law of conservation of mass, Richards (1931) developed an equation to represent flow through variably saturated media. Conservation of mass can be simplified as a function of water content in 3-D as the following function:

\* Corresponding author at: 2215 Raggio Parkway, Reno, NV 89512, USA.

E-mail addresses: [Michael.founds@gmail.com](mailto:Michael.founds@gmail.com), [m.founds@cbecoeng.com](mailto:m.founds@cbecoeng.com) (M.J. Founds).

$$\frac{d(\theta)}{dt} = -\frac{dq_x}{dx} - \frac{dq_y}{dy} - \frac{dq_z}{dz} - S \quad (1)$$

The change in water content over time is equal to the flux in each dimension and  $S$  represents any sources or sinks. Under homogeneous, isotropic conditions, vertical infiltration can be expressed by substituting the Darcy-Buckingham equation, yielding the Richards equation in 1D.

$$\frac{d(\theta)}{dt} = -\frac{d}{dz} \left( -K(h) \left( \frac{dh}{dz} + 1 \right) \right) - S \quad (2)$$

The  $K(h)$  term is the unsaturated conductivity as a function of matric potential. The term  $\frac{dh}{dz}$  represents capillarity and is a function of  $h$ . The “1” term is the simplification of  $\frac{dz}{dz}$  representing gravitational flow. The Richards equation is a nonlinear partial differential equation that models flow in the unsaturated zone.

Many analytical and semi-analytic expressions have been developed to model infiltration and recharge in the vadose zone. Some common approaches include the Green-Ampt model used to predict infiltration into homogeneous isotropic soils having a uniform moisture content (Ali et al., 2016; Green and Ampt, 1911; Selker et al., 1999; Selker and Assouline, 2017). Other approaches have relied on hydraulic conductivity and depth to the water table to solve for steady infiltration out of wells and spreading trenches (Bouwer, 2002; Hayek, 2014, 2016; Heilweil et al., 2015). Despite the active research on 1-D and 2-D infiltration over many decades, none of the analytic and semi-analytic expressions are designed to account for highly specific field conditions where there is unsteady infiltration into a complex geometry with a variably saturated heterogeneous soil profile. Pondered infiltration is affected by complex processes such as initial conditions, preferential pathways, or soil structure; these factors can be difficult to disentangle (Dohnal et al., 2016). While analytical infiltration equations have been developed to simplify Richards equation, practical applications of Richards equation often require numerical solutions (Radcliffe and Šimůnek, 2010).

### 1.3. Infiltration solutions using numerical methods

Hydrus simulations have recently been applied to solve a wide range of flow and contaminant transport problems within the vadose zone. Many recent studies have developed Hydrus 2D/3D models to compare agricultural practices, with a focus on optimizing water input while minimizing contaminants leaching to the groundwater (Akbar et al., 2015; Ebrahimian et al., 2012; Finch et al., 2008; Siyal et al., 2012; Wang et al., 2014). Hydrus is one of many numerical models developed to include multiple non-linear processes for complex applications involving flow and transport in variably saturated media (Šimůnek and Bradford, 2008). Hydrus 2D/3D numerically solves the Richards equation for variably saturated flow across a linear finite element mesh. Hydrus 2D/3D allows for representation of the following systems and processes: precipitation, evaporation, infiltration, runoff, lateral flow, soil water storage, capillary rise, deep groundwater recharge, hysteresis, root water uptake, and non-equilibrium flow (Šimůnek et al., 2012).

An operational strategy to implement MCs at the hillslope scale should consider the statistical frequency and intensity of rainfall, slope angle, and soil properties that affect the stability and infiltration capacity for MCs (Ziadat et al., 2014). Like any engineered structure, MCs need to be sized and spaced adequately for optimal function and cost effectiveness (Akroush et al., 2014; Oweis, 2016). Numerical modeling may provide a means to develop protocols for establishing effective MCs. The objective of this research is to use simple soil measurements to develop a predictive model of MC infiltration. The model was developed and tested using results from a field experiment that directly measured MC infiltration during a realistic rainfall-runoff scenario. This

research tests the ability of a 2-D Hydrus model to represent unsteady infiltration within several engineered MC structures that represent a realistic level of variability in hydrology, soils, and biological factors. Several methods are compared for parameterizing the model's soil properties using efficient field measurement techniques. By quantifying the ability of a numerical model to predict infiltration into MCs, this research creates a physically-based modeling framework to support effective rangeland restoration plans.

## 2. Materials and methods

### 2.1. Site description

Field investigations were carried out at a Bureau of Land Management (BLM) experimental research site at Bedell Flat located north of Reno, Nevada (119° 50' 5" W, 39° 51' 23" N). Soils of the study area are primarily of the Bedell Series, a coarse-loamy, mixed, superactive, mesic aridic argixeroll (Natural Resources Conservation Service, 2017). The underlying bedrock is typically within 1–2 m of depth and is a Cretaceous granodiorite. Average annual precipitation is 303 mm, most of which falls between November and March, and the mean annual temperature is 18 °C (PRISM, 2018). Eight MCs were created in two transects along the hillslope contour. The two transects were 50 m apart with the lower sites at the toe of the slope and the upper sites midway up the hillslope. The lower sites (L1-L4) had slopes of 5 to 8 percent, and the upper sites (U1-U4) ranged from 10 to 15% slope.

### 2.2. Micro-catchment design

The MCs are constructed by pulling the Vallerani plow along the contour of a hillslope. The plow includes a ripper to break up the soil profile and a hydraulically controlled curved metal blade that moves in a vertical wave motion from the surface to a depth of 30–50 cm within the soil. As the blade digs a 3.5–5 m long pit, it pushes the excavated soil downslope to form a semi-circular berm that is 20–30 cm high (Gammoh, 2011). Following construction, appropriate plant species are planted within each MC (Alshawahneh et al., 2011). Storm runoff flowing downslope is captured in the MC and infiltrates into the soil. The increased water content in the soil profile facilitates plant establishment and growth.

A digital 3-D model of a MC created by a Vallerani Plow in Jordan was used to design the shape of the Bedell Flat MCs. The MCs were constructed perpendicular to the slope direction by a small tractor pulling two offset plow shovels. The maximum depth reached by the tractor plow was approximately 20 cm, and each MC was manually shaped to represent dimensions that would be obtained using a Vallerani Plow. The upslope wall of the catchment was reshaped to an angle ranging from 80 to 90°. The downslope berm of the MCs had an angle of 35–45° on each side of the berm. The center of each catchment was excavated to a depth of 30–32 cm below the soil surface. To approximate the ripper of the Vallerani Plow System, a digging bar was used to break up the ground an additional 10–15 cm along a 20 cm wide furrow on the centerline of each MC. Each MC was approximately 350 cm long (perpendicular to slope) with a width at the surface of 150 cm and a depth of 30 cm.

A 3-D model of each MC was created using structure from motion (SfM) techniques to create relationships between stage, surface area, and volume. Eight fixed control targets placed around each site were surveyed with a Nikon NPR 352 total station to accurately project SfM 3-D models in space. Over fifty photos were taken with a Canon Rebel XTi and an iPhone 7 from various angles around the MCs. The set of photos from both cameras were input into Agisoft PhotoScan software. PhotoScan was used to align photos, build a dense point clouds, and create digital elevation models (DEMs) that were accurate to within 0.5 cm. The DEMs for each site were imported to Esri ArcMap 10.4.1 where the Surface Volume tool was used to capture the 3-D surface area

and volume across a range of depths. These datasets were imported into Microsoft Excel where polynomial relationships were applied to relate stage in each MC to soil surface area and water volume at a given depth.

### 2.3. Soil measurements

Soil samples were collected to complete laboratory measurements of bulk density and soil particle size distribution (PSD). PSD data can be used in pedotransfer functions to predict soil water retention and parameters and  $K_s$  (Rawls et al., 1982; Schaap et al., 2001; Wösten et al., 2001). The relationship between soil moisture ( $\theta$ ) and  $h$  for a given soil is highly dependent on soil texture and is widely used to predict soil hydraulic parameters based on the work of van Genuchten (1980) and Mualem (1976). The van Genuchten model uses three fitting parameters to define the shape of the soil water retention curve (SWRC) (van Genuchten, 1980).

$$Se(h) = 1 / [(-\alpha|h|)^m] \quad (3)$$

The term  $\alpha$  [ $L^{-1}$ ] is related to the inverse of the entry pressure. The  $n$  term is related to the pore size distributions. The  $m$  term is another shape factor which is usually set as a fixed relationship ( $m = 1/n$ ). The shape of the SWRC for a given soil is defined by the soil hydraulic parameters and allows for prediction of  $K(h)$  given a known pressure head or water content. The Rosetta computer program uses a neural network bootstrap method to estimate these parameters based on data from 2134 water retention samples and 1306  $K_s$  samples (Schaap et al., 2001). PSD samples were collected at upper and lower hillslope sites at five depth intervals, from the soil berm, and from the bottom of the pit following simulated rainfall (Fig. 2.1). Bulk density and PSD were measured in the Great Basin Rangelands Research Unit Soils Laboratory

of the USDA Agricultural Research Service. Bulk density was not included in this estimate since it was only collected at the soil surface.

Since PSD measurements do not account for soil structure, a direct measurement of saturated conductivity ( $K_s$ ) with the Guelph Permeameter (GP) was also tested. The GP can quickly measure  $K_s$  at varied depths using Richards and Laplace equations to obtain field-saturated hydraulic conductivity ( $K_{fs}$ ) and matric flux potential ( $\Phi_m$ ) for flow out of a cylindrical well (Reynolds and Elrick, 1985).  $K_{fs}$  is comparable to saturated conductivity ( $K_s$ ), but is assumed to include air entrapped in soil which typically occurs during field infiltration. GP solutions can be obtained using a single ponded height or two ponded heights within the well. The two ponded head method has been noted to be more accurate in controlled situations, but vertical heterogeneity of the soil profile can cause erroneous results (Elrick et al., 1989). Since infiltration rates varied with depth, the single ponded height was used. For the single ponded height method,  $K_{fs}$  can be calculated using the equation:

$$K_{fs} = \frac{Q}{\left[A + \left(\frac{B}{\alpha^*}\right)\right]} = \frac{CQ}{\left[\left(\frac{2\pi H^2}{C}\right) + \pi a^2 C + \frac{2H}{\alpha^*}\right]} \quad (4)$$

where  $H$  is the height of water ponded (cm),  $a$  is the radius of the well (cm),  $\alpha^*$  can be simplified as the ratio of  $K_{fs}/\Phi_m$ , and the  $C$  parameter represents the integral of pressure head across the well surface.  $C$  is dependent on the height of well water ( $H$ ), the radius ( $a$ ), and soil texture. The  $C$  parameter was calculated using the empirical function developed for structured loams and clays (Zhang et al., 1998). GP guidance provided by Soilmoisture, the manufacturer of the GP, suggest that this equation is applicable to most agricultural soils including unstructured medium and fine sands. GP measurements were taken on each side of the MCs (Fig. 2.1) at depths of 15 cm, 25 cm, 35 cm, 45 cm, 55 cm, and at 15 cm within the MC berm. All wells were created with a 6 cm diameter soil auger. Measurements were taken with the GP set to 10 cm of water pressure ( $H = 10$ ). Each well had a radius of 3 cm. The steady-state water level change was recorded at one-minute intervals until a steady rate of infiltration was achieved (i.e. three near-equal consecutive measurements of water level drop).

### 2.4. Micro-catchment instrumentation

Rainfall and concentrated flow (CF) experiments were carried out in August of 2017. Each of the eight MCs required a full day to complete the series of simulations, which were set up as shown in Fig. 2.2. The Walnut Gulch rainfall simulator (WGRS) (Paige et al., 2004) applied rainfall from a single oscillating boom to a  $2 \times 6.1$  m area that encompassed each MC. The WGRS was placed with the three nozzles aligned so that they spanned the length of the MC. Eight targets were placed around the MC to serve as fixed markers for a Nikon NPR 352 total station. A simulation control station was set up with a field computer that operated the WGRS and the two pressure transducers that were used to continuously measure ponded water depth. One transducer was an ISCO® bubbler that was connected to the custom-built stage recorder (SR) described below. The second was a vented KPSI 700 level transducer (KPSI) that was also placed within the SR. The SR device was a perforated, 8.8 cm diameter PVC pipe that was placed at the minimum elevation within the catchment. After rainfall experiments, a rill simulator was set up in an upslope position to deliver water for the concentrated flow experiments. The rill simulator is a stainless-steel box that is connected to a pump with a pressure regulator to control the flow rate. A digital flowmeter on the inlet to the rill simulator maintained a steady flow rate into the MC. Astroturf® (a plastic grass mat) was placed on the upslope edge of the MC to dissipate erosive forces of the water spilling out of the rill simulator.

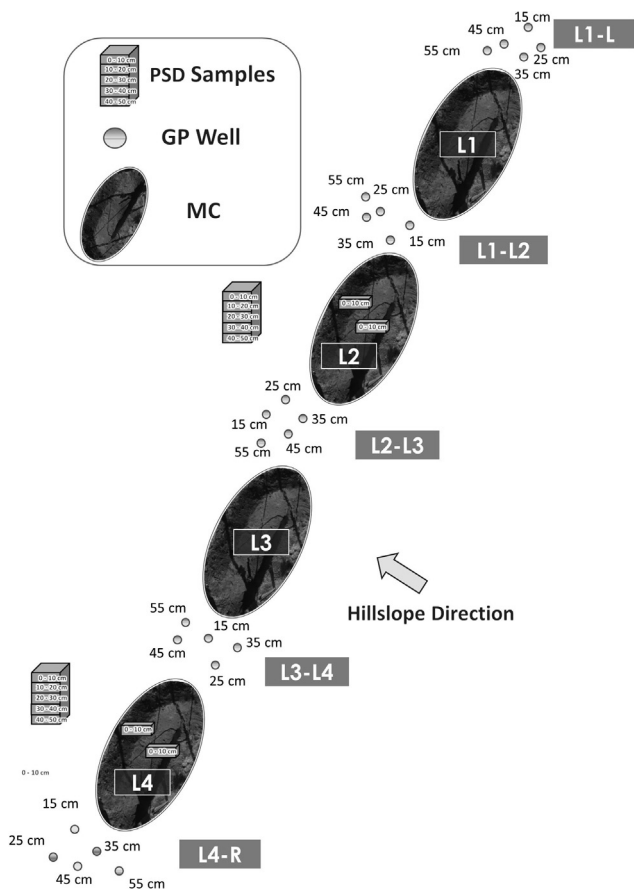


Fig. 2.1. Schematic overview of soil particle size distribution (PSD) sampling and Guelph Permeameter (GP) measurements for lower MCs. The sampling pattern was replicated at upper sites.

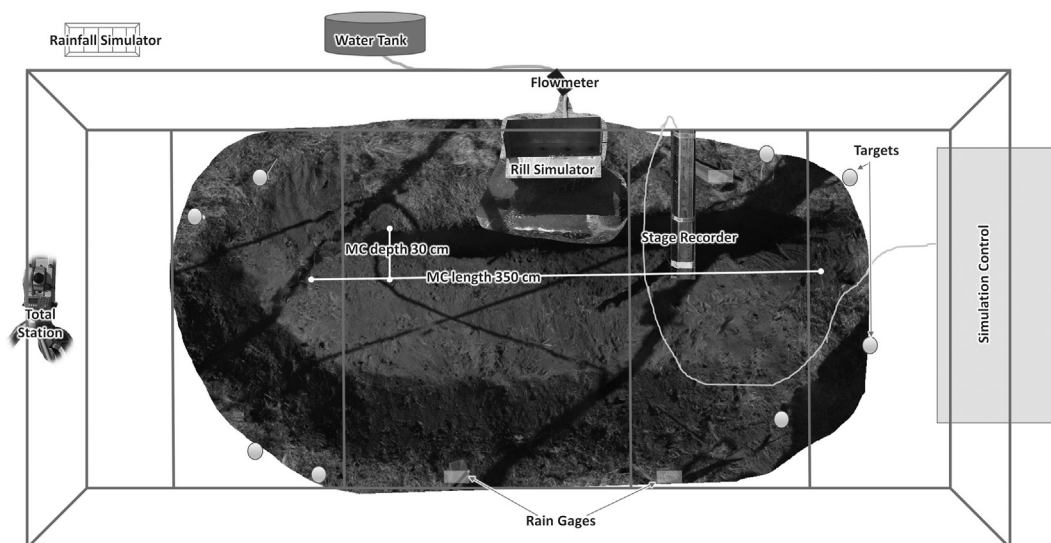


Fig. 2.2. MC instrumentation with WGRS, rill simulator, and SR.

## 2.5. Rainfall and concentrated flow experiments

This experiment represents a scenario where a hillslope received a large amount of rainfall followed by runoff entering the MC. A total of 2.5–5.0 cm of rainfall was delivered to each MC over two variable intensity and duration events. This was followed by a rill simulator that simulated runoff in the form of concentrated flow from upslope. After water overtopped the MC, the flow rate was maintained for at least 15 min. In the upper site, U2, a rodent hole was exposed near the bottom of the MC that caused rapid infiltration. This MC was removed from the study.

After the rill simulator was shut off and the water level dropped within the MC, the KPSI transducer recorded stage at one second intervals, and the ISCO bubbler recorded every 5 s. This continuous stage data from each MC was averaged to one-minute intervals to simplify the data and smooth out minor irregularities occurring over small intervals. Experiments were terminated after 120 min, or when the stage within the catchment dropped below 10 cm.

## 2.6. Hydrus model

A Hydrus model was developed and parameterized to mimic field experiments and predict volumetric flow rates.

### 2.6.1. Geometry and soil profile

A representative cross-section parallel to the hillslope was exported from the photogrammetric DEM for each MC. Two representative cross-sections were developed combining the lower sites (L1, L2, L3, L4) and the upper sites (U1, U3, U4) into a simplified geometry for each of the two hillslope positions. The upper sites were modeled with a 10% slope, and the lower sites with a 5% slope. A model domain was created that used the representative cross-sections parameterized by soil measurements made in the field. Additional points were added to project the modeled soil horizon boundaries at the correct slope across the model domain. The simple models of geometry for upper and lower sites were then imported into Hydrus. The model domain for upper and lower sites was approximately 500 cm wide by 500 cm tall. Seven soil layers were specified: 0–5 cm, 5–15 cm, 15–25 cm, 25–35 cm, 35–45 cm, > 45 cm, and the unconsolidated berm material (Fig. 2.3). The properties that were assigned to the berm were also specified for a wedge of soil at the bottom of the pit to represent the 10 cm of unconsolidated soil created with the digging bar.

Numerical solutions to the Richards equation require the model

domain to be discretized. Hydrus 2D/3D includes MESHGEN software which can be used to create a finite element (FE) mesh. The targeted FE size was set to 10 cm. Since the size of the FE mesh can be an important factor in determining infiltration (Dušek et al., 2009), the soil surface was refined to 1 cm discretization to improve model function across the boundary between soil and air. This also allowed for increased resolution in the model output across the area of interest.

### 2.6.2. Hydrologic boundary conditions

An atmospheric boundary condition was applied from the upslope edge of the model to slightly beyond the ridge of the berm. The atmospheric boundary allows for precipitation, evaporation, and for the time-varying head boundary that represents the ponded water surface.

Modeled evapotranspiration (ET) accounted for less than two percent of the flow budget over the short time period of this simulation, but is useful to consider in the model development for future model applications to longer simulations. Estimated ET rates for Bedell Flat were taken from a USGS publication with data for a comparable site nearby (Maurer et al., 2006). The selected dates for ET were chosen for our field site between August 1st–10th, yielding an average ET of 0.203 cm/day applied continuously over the simulation whenever the pressure head was negative. Hydrus rainfall inputs were set to represent the quantity and intensity of water added by the rainfall simulator. Each Hydrus model simulated 2.54 cm of rainfall occurring over the first 60 min across the atmospheric boundary condition. After the first 60 min of rainfall, no water inputs were added to the simulation until minute 200. This was to represent the time from when we operated the rainfall simulator to when the concentrated flow field simulations were initiated.

A time-varying head boundary was used to simulate the height of ponded water within each MC. Hydrus references the positive variable pressure head ( $h$ ) boundary to the minimum elevation in the boundary condition. The  $h$  values were derived directly from the SR readings and projected into each MC model for upper or lower sites. This was accomplished by establishing relationships between the observed maximum water level in the MC to the same level in the simplified Hydrus model. The result was a time-varying pressure head representing the exact height of ponded water specific to each site. The option to have an “atmospheric boundary condition when the specified nodal pressure head is negative” was also selected. This implies that any time that there is negative pressure head (no ponded water  $-h$ ) an atmospheric boundary condition is present. For the first 200 min of the simulation, the time-varying head boundary was set to  $-50$  cm. During

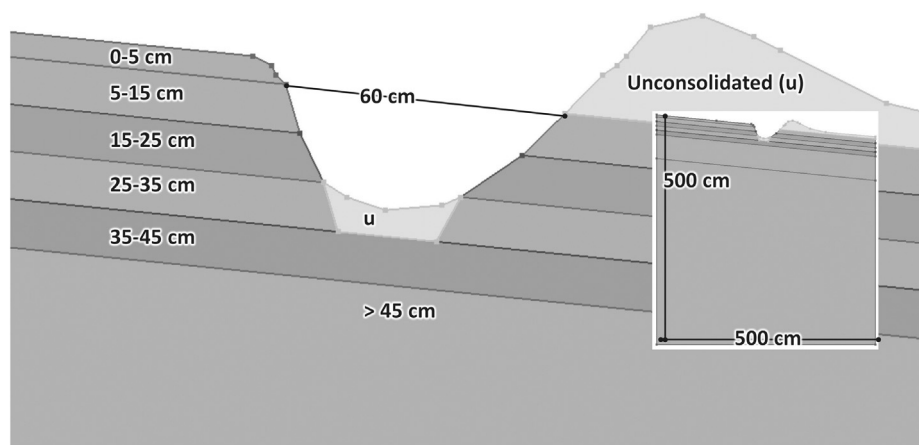


Fig. 2.3. Hydrus model geometry.

this period, precipitation and evaporation can occur across the entire atmospheric boundary. The values representing the water input into the catchment began at 200 min into the simulation, after which the observed height of ponded water was applied across the entire boundary. Areas with positive  $h$  have ponded water while areas with negative  $h$  retain an atmospheric boundary.

The Hydrus 2D model was set up in a vertical plane (XZ dimensions) to simulate water flow. The simulation was run for 400 min with an initial time-step of one minute. Forty output time steps were selected, with higher temporal resolution around the 200-minute mark when infiltration rates were compared to measured data. Initial model conditions were specified in pressure heads to match measured data. The shape of the water retention curve was defined by the van Genuchten – Mualem hydraulic model assuming no hysteresis, and water retention parameters were based on measured PSD data for each depth interval.

2.6.3. Conductivity profiles

The van Genuchten – Mualem hydraulic model requires inputs for both water retention parameters and  $K_s$ . Water retention parameters ( $Q_r$ ,  $Q_s$ , Alpha,  $n$ ,  $I$ ) were held constant for each simulation and were based on predictions from PSD data for each site (Table 3.1). Due to the high variability observed in the  $K_s$  data, four models of  $K_s$  with depth were used in simulations for each site:

**$K_s$  Profile 1:** PSD data was used in Rosetta to predict both water retention and  $K_s$  (Table 3.1). The pairs of PSD measurements taken at each hillslope position (upper vs lower) were averaged. The two  $K_s$

profiles distinguishing between upper and lower hillslope positions were used for respective MCs.

**$K_s$  Profile 2:** PSD data was used in Rosetta to predict both water retention and  $K_s$  (Table 3.1). The measurements were all averaged together regardless of hillslope position, and a single  $K_s$  profile was used for all MCs.

**$K_s$  Profile 3:** GP data for the two wells adjacent each MC for the entire soil profile were averaged for each depth interval (Table 3.2).

**$K_s$  Profile 4:** The maximum GP measurement from each depth interval is selected from the separate GP datasets for the lower sites versus upper sites. The two maximum values from the upper and lower sites at each depth interval are then averaged (Table 3.3). The model uses a single averaged  $K_s$  profile for all sites, regardless of hillslope position.

Running the seven MC models with four  $K_s$  profiles yielded 28 Hydrus solutions to compare to measured infiltration rates. The period of interest for this study was the 30 min after inflow to each MC was stopped, allowing for observation of hydrologic function while the stage within the MC is near the maximum.

2.6.4. Calculating infiltration

A 2-D model was developed in Hydrus to predict the infiltration rates for each MC. Based on field measurements, the soil profile was modeled with seven layers with distinct soil properties (Fig. 2.4a). The model yielded a velocity distribution across the saturated area (Fig. 2.4b). The boundary output information for relevant time steps was averaged across each depth interval to create a velocity profile with

Table 3.1  
PSD data analysis and Rosetta Lite 1.1 prediction of hydraulic parameters.

Measured PSD Data			Rosetta Lite 1.1 Prediction of Soil Water Retention Parameters and $K_s$							
Site	Depth Interval	% Clay	% Silt	% Sand	Residual Water Content ( $Q_r$ ) [cm <sup>3</sup> /cm <sup>3</sup> ]	Saturated Water Content ( $Q_s$ ) [cm <sup>3</sup> /cm <sup>3</sup> ]	Alpha [1/cm]	$n$ [-]	$K_s$ [cm/min]	
Lower	<b>Avg Lower</b>	8.7	15.1	74.9	0.042	0.384	0.038	1.5	0.042	
	0–10 cm	3.1	15	81.5	0.037	0.389	0.044	1.8	0.084	
	10–20 cm	6.2	13.8	79.2	0.041	0.385	0.04	1.6	0.061	
	20–30 cm	11.4	15.9	71.3	0.046	0.383	0.035	1.4	0.031	
	30–40 cm	11.9	15.6	70.7	0.046	0.383	0.034	1.4	0.029	
	40–50 cm	10.9	15	71.9	0.045	0.383	0.035	1.4	0.033	
	Basin	9.2	17.4	72.2	0.042	0.385	0.037	1.5	0.037	
	Berm	5.8	16	77.7	0.039	0.386	0.041	1.6	0.056	
	Upper	<b>Avg Upper</b>	4.5	9.5	85.7	0.046	0.427	0.039	2	0.207
		0–10 cm	2.2	7.9	89.7	0.045	0.384	0.039	2.6	0.235
10–20 cm		3.4	10.7	85.7	0.042	0.385	0.04	2.1	0.13	
20–30 cm		4.4	10.2	85.1	0.044	0.383	0.039	2	0.116	
30–40 cm		6.2	10.6	82.8	0.044	0.382	0.038	1.8	0.084	
40–50 cm		8.2	6.4	84.7	0.051	0.377	0.033	1.9	0.093	
Basin		4	11.1	84.1	0.042	0.385	0.04	2	0.112	
Berm		3.1	10.4	85.6	0.042	0.386	0.041	2.1	0.131	

**Table 3.2**  
GP Kfs results averaged from wells on each side of a MC and within berm (cm/min).

Depth (cm)	L1	L2	L3	L4	U1	U3	U4	Lower Avg	Upper Avg	All Avg
5–15	0.037	0.036	0.031	0.036	0.061	0.100	0.097	0.035	0.086	0.057
15–25	0.014	0.012	0.014	0.016	0.053	0.052	0.072	0.014	0.059	0.033
25–35	0.013	0.005	0.002	0.001	0.020	0.002	0.016	0.005	0.013	0.008
35–45	0.018	0.005	0.003	0.001	0.012	0.007	0.008	0.007	0.009	0.008
45–55	0.006	0.006	0.006	0.004	0.012	0.001	0.004	0.005	0.006	0.005
Berm	0.137	0.056	0.318	0.092	0.121	0.235	0.158	0.151	0.171	0.160

**Table 3.3**  
Maximum GP Kfs values for upper, lower, and average of the two hillslope positions at each depth interval (cm/min).

Depth (cm)	Lower Max	Upper Max	Average Max
5–15	0.114	0.156	0.135
15–25	0.069	0.127	0.098
25–35	0.065	0.095	0.080
35–45	0.016	0.012	0.014
45–55	0.004	0.013	0.008
Berm	0.169	0.125	0.147

flow rate ( $Q_{1\text{-cm interval}}$ ) of water infiltrating over a 1-cm interval that can be summed to yield a volumetric flow rate ( $Q_{\text{sum}}$ ) [ $L^3T^{-1}$ ] for a given time step.

$$Q_{\text{sum}} = \sum_{MCbottom}^{SoilSurface} Q_{1\text{-cminterval}}$$

2.6.5. 2-D versus 3-D

All models described previously were developed as 2-D vertical planes. This was done to create a cross-section that represented MC geometry. However, the vertical plane model ignores that water fluxes into the MC occur in 3-D. The 2-D profile of the Hydrus model does not account for the additional 3-D soil volume that exists at the curved ends of the MC. This could be conceptualized using a 3-D Hydrus model, but that would have the disadvantage only being applicable a unique modeled geometry. Using the 2-D Hydrus model, flow rates can be predicted for a MC of any length using the stage to surface area relationship. Hydrus can conceptualize 3-D flow as a 2-D axisymmetric model, allowing the entire model domain to be rotated along the z-axis. The change in velocity profile between a 2-D vertical plane model and a 2-D axisymmetric model for the characteristic MC geometry was tested for a common MC shape. The difference between 2-D vertical plane and 2-D axisymmetric flow is dependent on the radius of the boundary being rotated. While MCs are not circular, the effective radius of a MC was calculated as:

$$EffectiveRadius = \sqrt{\frac{VMCSurfaceArea}{\pi}}$$

For an average MC nearly full, the average effective radius was 80 cm. The MC Hydrus model was modified to have only one side that extends 80 cm and could be rotated along the z axis. The new geometry based on effective radius was run as a 2-D vertical plane model, just like each other MC model, and then run as an axisymmetric model.

3. Results

3.1. Soils analysis

The average of the samples of PSD at upper and lower MCs, along with Rosetta predictions of water retention parameters and  $K_s$ , are presented in Table 3.1. The upper sites had lower  $K_s$  estimates due to the higher silt and clay content, which generally increased below 20 cm. The average bulk densities at the soil surface were 1.31  $g/cm^3$  and 1.37  $g/cm^3$  for upper and lower sites respectively. Table 3.2 presents GP data averaged from each side of a MC. All  $K_{fs}$  values were calculated using the single head measurement method with Eq. (1). In general, upper sites had higher  $K_{fs}$  values compared to lower sites at each depth interval. This was consistent with predictions based on the PSD data displayed in Table 3.1. In upper and lower sites  $K_{fs}$  values were highest in the interval of 5–15 cm. The  $K_{fs}$  values below 25 cm were often a fraction of the surface  $K_{fs}$  values. Table 3.3 presents the maximum GP measurement at each depth interval averaged across upper and lower sites.

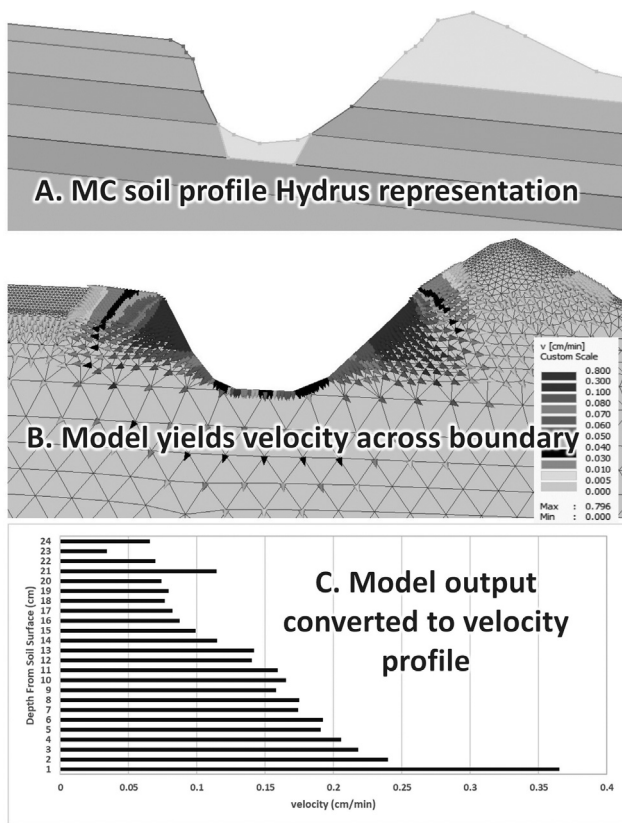


**Fig. 2.4.** MC predictive infiltration model to yield velocity profile with soil depth.

soil depth (Fig. 2.4c).

The velocity profile provides useful information to convert 1-D flux of water  $q$  [ $LT^{-1}$ ] into volumetric flow rate ( $Q$ ) [ $L^3T^{-1}$ ] using the relationship between stage and surface area. Simulated fluxes were compared to measured infiltration rates at six 5-minute intervals after the inflow into the MC ended. The output velocity values ( $q$ ) were averaged within each 1-cm interval across the ponded boundary for a given time step and model run. The 3-D surface area of the corresponding 1-cm interval for each MC was calculated, and each  $q$  was multiplied by the corresponding surface area. This yielded a volumetric

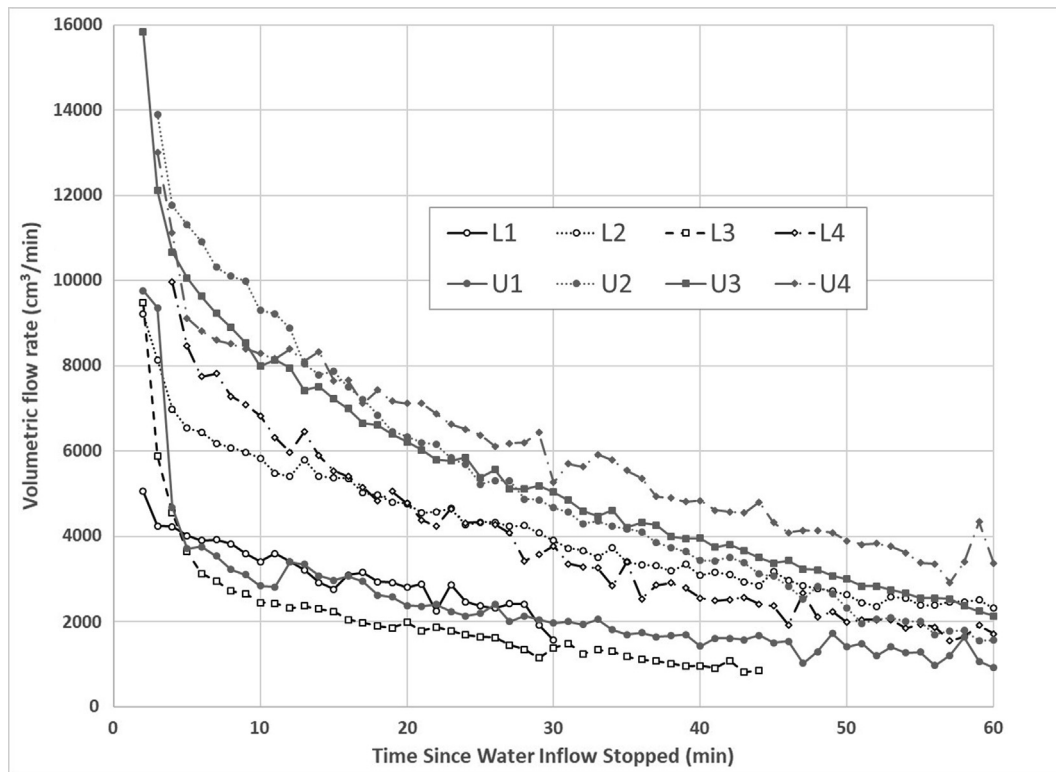


Fig. 3.1. Volumetric flow rate for the 60 min after water inflow was stopped.

3.2. Measured infiltration

After inflow was turned off, measured changes in stage were related to catchment volume using polynomial relationships to calculate infiltration rates. The time-varying volumetric flow rates for each MC are presented in Fig. 3.1. In each site the volumetric flow rate was highest directly after the inflow to the MC was stopped and would decrease rapidly over the first ten minutes. After the initial rapid infiltration, the volumetric flow rates decreased linearly. Upper sites, except for U1, had faster infiltration rates than the lower sites.

3.3. Model outputs

The final model water balance errors ranged from 0.014% to 0.031%. Fig. 3.2 presents pressure head (Fig. 3.2a), water content (Fig. 3.2b), and velocity (Fig. 3.2c) for a typical simulation of the L1 MC at 255 min into the simulation. At this period, there is no inflow into the MC and the water level is falling. The velocity vectors ( $q$ ) (Fig. 3.2c) were used to calculate infiltration.

3.4. Simulated infiltration

The modeled volumetric flow rates were compared to the field measured volumetric flow rates displayed in Fig. 3.1. Each of the four sets of conductivity data were used to run the model and yield a separate prediction. Fig. 3.3 displays an example of observed and modeled results for  $K_s$  Profiles 1–4 at sites L3 and U4. Sites L3 and U4 were selected because they are representative of average infiltration dynamics occurring at the lower and upper hillslope positions respectively. Fig. 3.4 graphically compares the percent error  $[(\text{observed} - \text{modeled})/\text{observed}]$  for each site, timestep and conductivity profile. The results for each site are displayed using average error, in which two sites with opposite magnitude of error offset each other. The black bars indicate underprediction of results while the grey bars indicate an overprediction of observed flow rates by the model. Over the 6 periods

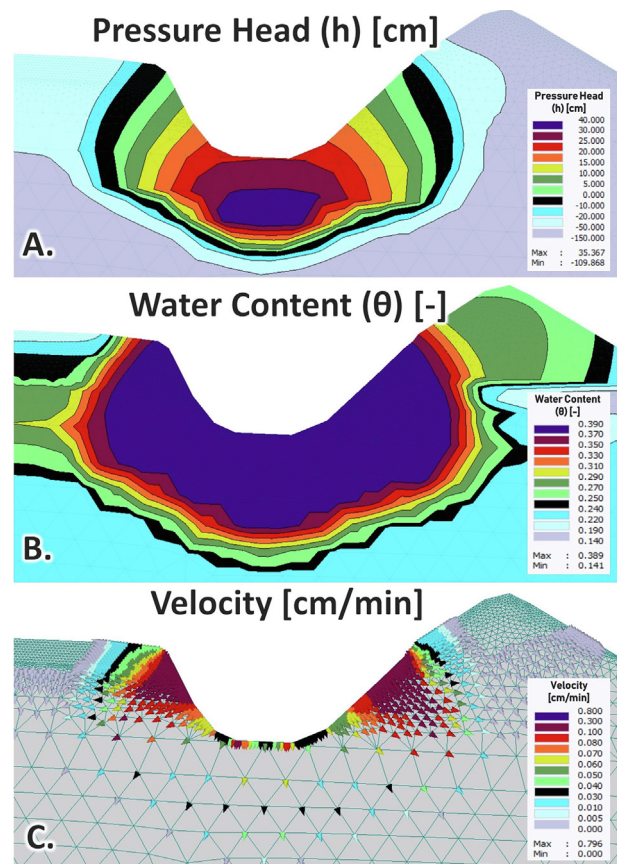


Fig. 3.2. Hydrus output for L1 at 255 min displaying pressure, water content, and velocity.

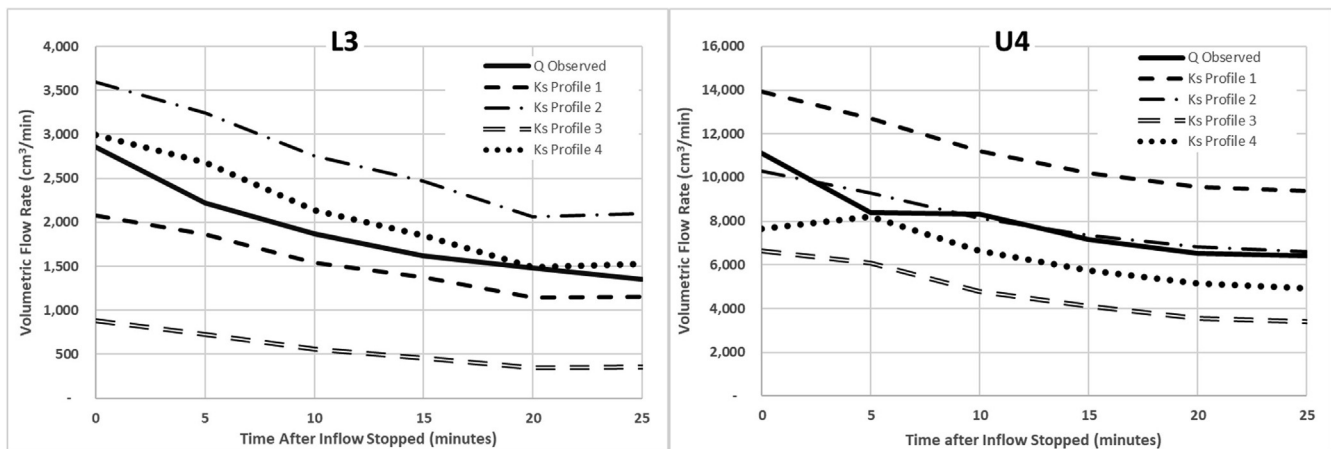


Fig. 3.3. Measured vs. modeled volumetric flow rates for L3 and U4 with Ks Profile 1–4.

of the simulation for each site and  $K_s$  profile, most models predicted volumetric flow rates with a similar size of error. This suggests that the models capture the general variation of fluxes within MCs over the 30-minute model period. However, the magnitude of error changed between sites, and with different  $K_s$  profile data. The comparison between all 2-D vertical results and the axisymmetric model showed that 2-D results slightly underpredict flow rates. Axisymmetric models had an average of 11% greater velocity ( $q$ ) and 8% larger volumetric flow rate.

#### 4. Discussion

The variation in error seen in Fig. 3.3 across each  $K_s$  profile provide insight into the infiltration dynamics at each site.  $K_s$  Profile 1 and 2 both rely on PSD data with pedotransfer functions, and consequently have similar patterns in observed vs. predicted results.  $K_s$  profile 3 and 4 both relied on GP measurements, with the difference being that  $K_s$  profile 4 used the maximum measurements from each depth interval. The physical mechanisms underlying the accuracy of predictions using each  $K_s$  Profile are explored here.

For  $K_s$  Profile 1 that averaged two measurements for the upper and two measurements for the lower sites, the upper sites overpredicted flow rates while the lower sites underpredicted flow rates. The average error for  $K_s$  Profile 1 was off by 34%. The absolute error, calculated as the absolute value of each result averaged across the site, was off by 75%. Average error allows bias to be canceled out across sites. Models run with  $K_s$  Profile 2 also had an average error of overpredicting by 34%, but the absolute error was reduced to 47%. Separating upper and lower sites did worse than  $K_s$  Profile 2 that used the same conductivity profile for the two hillslope positions. Additional soil samples would need to be taken to determine if the variability between upper and lower sites was an indication of physical differences between sites, or just a result of under-sampling. The particle size distribution dataset that was used to generate the conductivity values relied on pedotransfer functions and were not direct measurements of  $K_s$ . As Schaap et al. (2001) noted regarding the Rosetta software, including more predictor variables than soil particle size distribution yields more accurate  $K_s$  estimates. Furthermore, pedotransfer functions are likely not an accurate indicator of  $K_s$  at the point scale since they do not consider soil structure (Wösten et al., 2001). Another study looking at systematic field-scale variability of  $K_s$  on an artificially constructed ecosystem found that pedotransfer functions underpredicted  $K_s$  by an order of magnitude and were a major source of uncertainty in hydrological modeling (Gwenzi, 2011). The soils at the study area are natural, but soil disturbances during construction surely altered the soils hydrologic properties. While pedotransfer functions did produce relatively unbiased solutions for some sites, a direct measure of  $K_s$  using a GP or double ring infiltrometer is likely more representative of field-scale

conditions. Here the GP was selected for its improved ability to operate on a slope and at multiple depth intervals.

When the model is parameterized by  $K_s$  Profile 3 (GP data), the flow rate in the lower sites was underpredicted by an average of 72%, while the upper sites were on average 29% lower than observed data. The severe underestimation of volumetric flow rate from these direct measurements can be attributed to three reasons. First, uniform flow models do not consider the more complex geometry of flow paths in the soil. Preferential flow paths are observed in almost all soils, yet are rarely accounted for in simulation models (Germann and Hensel, 2006). Fractures in the soil profile, or a structured soil, can provide pathways for water to move more rapidly than would be predicted by the Richards Equation. The amount of preferential flow is dependent on the soil and geology, and in some cases can account for the majority of recharge (Sukhija et al., 2003). Another study exploring spatial and temporal variation in ponded infiltration using numerical models represented the proportion of preferential flow ranging from 3 to 40% (Dohnal et al., 2016). Assuming this is the only reason for underestimating flow, 50% of flow across all sites would be through preferential pathways.

Second, the GP measurements do not accurately represent the MC due to differences in scale between the GP measurements and the MC. In the much larger MC, water will flow along preferential flow paths that would not necessarily be sampled by the narrow well of GP measurements, since access to macropores is limited. Many researchers have noted the challenges in measuring  $K_s$  because it is highly dependent on observational scale (Chappell and Lancaster, 2007; Brooks et al., 2004; Zobeck et al., 1985). The small surface area of the average GP measurements relative to the MC (approximately 1:30 for surface area, 1:150 for volume) may explain underprediction of flow rates when the model is parameterized with  $K_s$  Profile 3, since the smaller well may have less opportunity to encounter preferential flow paths. Third, the model is not fully considering 3-D flow. The difference between the 2-D vertical plane and the axisymmetric model for L1 resulted in an average of 11% greater velocity ( $q$ ) across the boundary for axisymmetric flow. This resulted in an 8% increase in volumetric flow rate, indicating a limitation with the 2-D model. However, the MCs constructed in this study were of relatively short length compared to most field implementations, and we would expect this discrepancy to be mitigated for a longer trough where the 2D profile was representative of a larger proportion of the pit.

While the scientific literature has previously documented issues in accounting for preferential flow and observational scale affecting  $K_s$  measurements, the results of this study reinforce the importance of accounting for these factors when applying GP measurements to the scale of a MC. The difference observed between upper and lower sites is likely related to the first two reasons provided above. Preferential flow

Site	K <sub>s</sub> 1: PSD (split)	K <sub>s</sub> 2: PSD (avg)	K <sub>s</sub> 3: GP	K <sub>s</sub> 4: GP (max)
26		-18	55	3
17		-34	48	4
12		-42	54	-6
14		-41	51	6
7		-53	51	3
-9		-79	51	-24
58		29	83	60
66		40	86	62
64		34	85	57
57		20	83	49
54		13	83	46
58		21	85	51
27		-26	69	-5
16		-46	67	-21
17		-47	70	-15
15		-52	72	-14
23		-39	76	-1
14		-55	74	-13
55		26	78	38
53		20	79	34
57		25	82	42
52		14	82	36
59		27	86	47
52		13	85	40
-162		-95	-9	-69
-133		-72	8	-45
-152		-83	5	-51
-175		-97	4	-55
-236		-140	-17	-90
-183		-100	9	-47
-170		-122	3	-60
-171		-94	2	-58
-166		-89	17	-44
-183		-100	27	-43
-180		-96	39	-32
-142		-68	54	-6
-25		7	40	31
-51		-11	27	2
-34		2	43	20
-42		-2	43	20
-47		-5	45	21
-46		-3	47	24
	-34.2	-33.7	50.5	0.0

Fig. 3.4. Percent error for all K<sub>s</sub> Profiles. Negative values (grey bars) indicate the model overpredicted observed results. Positive values (black bars) indicate the model underpredicted observed results.

may occur due to soil structural cracks, roots, soil management, or faunal activity (Angulo-Jaramillo et al., 2016). The higher flow rates relative to measured conductivity values in the lower sites could indicate the presence of increased preferential flow paths. One cause for this disparity could be the difference in biological activity in the upper and lower sites. The plants in the lower site may have had a deeper rooting depth, creating flow paths at greater depth within the soil. Rodent holes and ant hills were frequent within the study area, and more prevalent in the lower transect of MCs. Even if a MC did not directly intersect any subsurface animal holes, the water could have been accessing these larger flow paths as it moved laterally and into the subsurface.

K<sub>s</sub> Profile 4 (Max GP values) was intended to better account for preferential flow, since the maximum estimated K<sub>s</sub> from GP

measurements might be a more scalable measurement to predict flow in larger MCs (assuming no significant issues with burrows, etc.). The Hydrus model with K<sub>s</sub> Profile 4 underestimated by 20% for lower sites and overestimated by 30% for the upper sites. Of the four K<sub>s</sub> models, K<sub>s</sub> Profile 4 made the least biased prediction of flow with an average error of less than 1%. While these results provide a useful model to represent the MC function at the study areas, the exact number of measurements required to make a representative K<sub>s</sub> profile will be specific to each soil. Efforts to predict ponded infiltration in MCs should consider using a higher percentile value from the distribution of GP measurements to account for the infiltration processes not represented in the numerical model.

Given that the goal of this research was to develop protocols that will allow for MC establishment at the hillslope scale, the four K<sub>s</sub>

Profiles considered in this study represent a useful range on inputs for forward numerical model simulation to represent a range of infiltration dynamics observed in the field. Inverse modeling techniques have been demonstrated to improve parameterization of vadose zone models. This approach has been used by Wang et al. (2003) to evaluate flow into a stratified vadose zone, Xu et al. (2017) to more accurately predict soil moisture with limited soils information, and Zhang et al. (2016) to characterize the subsurface hydraulic properties in clusters optimized by inversion. Inverse modeling could provide an additional mechanism to improve modeling results, although this may be beyond the scope of an operational strategy to survey micro-catchments at other locations.

By default, Hydrus uses the uniform flow model, where the Richards Equation dictates the rate at which water can flow through the pore space within an impermeable matrix. Many nonequilibrium flow models have been created in Hydrus to address increasingly complex representation of physical and chemical flow through a model domain. While more complex models may do a better job representing the physical processes such as preferential flow within the soil, it can be difficult to directly measure many of the parameters required to run non-equilibrium models (Šimůnek and van Genuchten, 2008). The simultaneous processes involved in ponded infiltration can make it difficult to confidently understand whether flow rates were a result of preferential pathways, or another variable such as height of ponded water (Dohnal et al., 2016). In our study area, use of the  $K_s$  Profile 4 provided an unbiased solution. Future research should investigate what range of GP measurements best characterize ponded infiltration into MCs with different soil conditions. It is reasonable to assume that this model would also be an effective model for similar soils MC geometries. The experiments on the seven MC help to characterize the range of infiltration scenarios that can be expected when MC are developed at the hillslope scale and will be useful in planning MC size and spacing for future restoration efforts.

This research effort predicted infiltration in MCs based on 2-D Hydrus simulations for a single high-intensity event. Assouline and Mualem (2002, 2006) studied how high-intensity rainfall can cause surface sealing in semiarid catchments and affect the spatial variability of infiltration. Another study on small catchments designed for water harvesting noted the impact of fine sediments from upslope being transported into the MC and altering the texture of the surface soils (Previati et al., 2010). Accumulation of fine sediment at the bottom of each MC was also observed following rainfall simulations in our study. The combination of surface sealing and additional input of fine sediment into the MCs add complexity in predicting flow rates. The wide array of physical processes taking place during unsteady MC infiltration make it necessary to carry out field experiments instead of solely relying on modeling results.

Future work could adapt simulations to more complex scenarios to answer pertinent research questions, such as representing MC function resulting from weather patterns and plant growth over a seasonal time scale. The Hydrus model could also be used in conjunction with other physically based erosion models. This would allow land managers to test potential configurations of MCs at the hillslope scale for minimizing erosion while controlling costs. The 2-D process developed in this paper is applicable far beyond infiltration into MCs. Infiltration could be predicted for a large system such as a ditch or wetland, where a 3-D Hydrus model would be computationally prohibitive.

## 5. Conclusion

Rainfall and concentrated flow experiments were designed to represent a rainfall scenario where runoff enters MCs created by a Vallerani® Plow. A modeling process using Hydrus 2D/3D was developed to predict volumetric flow rates when the MCs were nearly full. The magnitude of predicted infiltration was highly dependent on the estimate of  $K_s$ . Sources of error likely resulted from preferential flow paths not represented in the model, differences in scale between the

permeameter wells and the MCs, and the difference between 2-D and 3-D flow. Use of the maximum GP  $K_s$  data at each depth averaged for upper and lower sites was the least biased representation of the flow processes taking place within a MC. When considering restoration opportunities with MCs in a new location, it is important to consider that a higher range of GP measurement will likely be a better representation of the multitude of hydrologic processes involved in unsteady ponded infiltration. The method of using Hydrus to yield a velocity profile was an effective way to predict infiltration into the unsaturated zone. The modeling process was developed to evaluate the efficacy of hillslope restoration using the Vallerani system and currently provides volumetric flow rates at each level of ponded water within a MC. Event-based flow and erosion models could be used to create a time series of incoming discharge into a MC based on the upslope conditions which could be applied in Hydrus to determine infiltration dynamics. This would increase the model's utility as a planning tool to determine whether a configuration of MCs on a hillslope are of adequate length and spacing to infiltrate runoff from a storm event. From an erosion management perspective, this is a critical step in designing a successful restoration strategy. Furthermore, the positive impacts of a mitigation strategy could be quantitatively compared across sites, or to other restoration strategies.

## Declaration of Competing Interest

The authors declared that there is no conflict of interest.

## Acknowledgement

This research was supported through a Cooperative Agreement (59-2060-6-001) with the Agricultural Research Service of the United States Department of Agriculture that is in turn funded through Agreement 60-5370-4-001 from the U.S. Bureau of Land Management. Special thanks for support from the team at the ARS Great Basin Rangelands Research Unit in Reno, Nevada.

## References

- Akbar, G., Raine, S., McHugh, A.D., Hamilton, G., 2015. Managing lateral infiltration on wide beds in clay and sandy clay loam using Hydrus 2D. *Irrig Sci.* <https://doi.org/10.1007/s00271-014-0458-9>.
- Akroush, S., Shideed, K., Bruggeman, A., 2014. Economic analysis and environmental impacts of water harvesting techniques in the low rainfall areas of Jordan. *J. Agric. Resour. Gov. Ecol. Int.* <https://doi.org/10.1504/ijarge.2014.061040>.
- Ali, S., Islam, A., Mishra, P.K., Sikka, A.K., 2016. Green-ampt approximations: a comprehensive analysis. *J. Hydrol.* <https://doi.org/10.1016/j.jhydrol.2016.01.065>.
- Alshawahneh, N., Saoub, H., Oweis, T., Haddad, N., 2011. Impact of micro-catchment water harvesting on plant diversity in Jordan Badia rangelands. *Meet. Chall. Sustain. Dev. drylands under Chang. Clim. – Mov. from Glob. to local*, Proc. Tenth Int. Conf. Dev. Drylands, 12-15 December 2010, Cairo, Egypt.
- Angulo-Jaramillo, R., Bagarello, V., Iovino, M., Lassabatere, L., 2016. Infiltration measurements for soil hydraulic characterization. *Infiltrat. Measurment. Soil Hydraul. Character.* <https://doi.org/10.1007/978-3-319-31788-5>.
- Assouline, S., Mualem, Y., 2006. Runoff from heterogeneous small bare catchments during soil surface sealing. *Water Resour. Res.* <https://doi.org/10.1029/2005WR004592>.
- Assouline, S., Mualem, Y., 2002. Infiltration during soil sealing: The effect of areal heterogeneity of soil hydraulic properties. *Water Resour. Res.* <https://doi.org/10.1029/2001WR001168>.
- Bouwer, H., 2002. Artificial recharge of groundwater: Hydrogeology and engineering. *Hydrogeol. J.* <https://doi.org/10.1007/s10040-001-0182-4>.
- Brooks, E.S., Boll, J., McDaniel, P.A., 2004. A hillslope-scale experiment to measure lateral saturated hydraulic conductivity. *Water Resour. Res.* <https://doi.org/10.1029/2003WR002858>.
- Buckingham, E., 1907. Studies on the Movement of Soil Moisture. *Bur. Soils–Bull No. 38.* <https://doi.org/10.1017/CBO9781107415324.004>.
- Chappell, N.A., Lancaster, J.W., 2007. Comparison of methodological uncertainties within permeability measurements. *Hydrol. Process.* <https://doi.org/10.1002/hyp.6416>.
- Darcy, H., 1856. Détermination des lois d'écoulement de l'eau à travers de sable. *Les Fontaines Publiques de La Ville de Dijon.*
- Dohnal, M., Vogel, T., Dusek, J., Votrubova, J., Tesar, M., 2016. Interpretation of ponded infiltration data using numerical experiments. *J. Hydrol. Hydromechanics.* <https://doi.org/10.1515/johh-2016-0020>.

- Dušek, J., Dohnal, M., Vogel, T., 2009. Numerical analysis of ponded infiltration experiment under different experimental conditions. *Soil Water Res.* 4.
- Ebrahimiyan, H., Liaghat, A., Parsinejad, M., Abbasi, F., Navabian, M., 2012. Comparison of one- and two-dimensional models to simulate alternate and conventional furrow fertigation. *J. Irrig. Drain. Eng.* [https://doi.org/10.1061/\(asce\)ir.1943-4774.0000482](https://doi.org/10.1061/(asce)ir.1943-4774.0000482).
- Elick, D.E., Reynolds, W.D., Tan, K.A., 1989. Hydraulic conductivity measurements in the unsaturated zone using improved well analyses. *Groundw. Monit. Remediat.* <https://doi.org/10.1111/j.1745-6592.1989.tb01162.x>.
- Finch, S.D., Radcliffe, D.E., West, L.T., 2008. Modeling trench sidewall and bottom flow in on-site wastewater systems. *J. Hydrol. Eng.* [https://doi.org/10.1061/\(asce\)1084-0699\(2008\)13:8\(693\)](https://doi.org/10.1061/(asce)1084-0699(2008)13:8(693)).
- Gammoh, I.A., 2011. Double furrow with raised bed-A new improved mechanized water-harvesting technique for large-scale rehabilitation of arid rain-fed areas. *Soil Tillage Res.* <https://doi.org/10.1016/j.still.2011.01.003>.
- Gammoh, I.A., Oweis, T.Y., 2011. Performance and adaptation of the vallerani mechanized water harvesting system in degraded badia rangelands. *J. Environ. Sci. Eng.* 5, 1370–1380.
- Germann, P.F., Hensel, D., 2006. Poiseuille flow geometry inferred from velocities of wetting fronts in soils. *Vadose Zo. J.* <https://doi.org/10.2136/vzj2005.0080>.
- Green, W.H., Ampt, G., 1911. Studies on soil physics: I. Flow of air and water through soils. *J. Agric. Sci.*
- Gwenzi, W., Hinz, C., Holmes, K., Phillips, I.R., Mullins, I.J., 2011. Field-scale spatial variability of saturated hydraulic conductivity on a recently constructed artificial ecosystem. *Geoderma.* <https://doi.org/10.1016/j.geoderma.2011.06.010>.
- Hayek, M., 2016. Analytical solution to transient Richards' equation with realistic water profiles for vertical infiltration and parameter estimation. *Water Resour. Res.* <https://doi.org/10.1002/2015WR018533>.
- Hayek, M., 2014. Water pulse migration through semi-infinite vertical unsaturated porous column with special relative-permeability functions: Exact solutions. *J. Hydrol.* <https://doi.org/10.1016/j.jhydrol.2014.06.001>.
- Heilweil, V.M., Benoit, J., Healy, R.W., 2015. Variably saturated groundwater modelling for optimizing managed aquifer recharge using trench infiltration. *Hydrol. Process.* <https://doi.org/10.1002/hyp.10413>.
- Malagnoux, M., 2008. Degraded arid land restoration for afforestation and agro-silvo-pastoral production through new water harvesting mechanized technology. *Fut. Drylands.* [https://doi.org/10.1007/978-1-4020-6970-3\\_30](https://doi.org/10.1007/978-1-4020-6970-3_30).
- Maurer, D.K., Berger, D.L., Tumbusche, M.L., Johnson, M.J., 2006. Rates of evapotranspiration, recharge from precipitation beneath selected areas of native vegetation, and streamflow gain and loss in Carson Valley, Douglas County, Nevada, and Alpine County, California. *U.S. Geol. Surv. Sci. Investig. Rep.* 2005–5288.
- Mualem, Y., 1976. A new model for predicting the hydraulic conductivity of unsaturated porous media. *Water Resour. Res.* <https://doi.org/10.1029/WR012i003p00513>.
- Oweis, T.Y., 2016. Rainwater harvesting for restoring degraded dry agro-pastoral ecosystems: a conceptual review of opportunities and constraints in a changing climate. *Environ. Rev.* <https://doi.org/10.1139/er-2016-0069>.
- Natural Resources Conservation Service, 2017. United States Department of Agriculture. *Bedell Series Official Soil Series Descriptions.* <https://soilseries.sc.egov.usda.gov/osdname.aspx> (accessed 20 March 2018).
- Oweis, T.Y., Karrou, M., Ziadat, F., F., A., 2011. Rehabilitation and integrated management of dry rangelands environments with water harvesting. *International Center for Agricultural Research in the Dry Areas, Report no. 9, Aleppo, Syria*, 208 pp.
- Paige, G.B., Stone, J.J., Smith, J.R., Kennedy, J.R., 2004. The walnut gulch rainfall simulator: a computer-controlled variable intensity rainfall simulator. *Appl. Eng. Agric.*
- Previatei, M., Bevilacqua, I., Canone, D., Ferraris, S., Haverkamp, R., 2010. Evaluation of soil water storage efficiency for rainfall harvesting on hillslope micro-basins built using time domain reflectometry measurements. *Agric Water Manag.* <https://doi.org/10.1016/j.agwat.2009.11.004>.
- PRISM Climate Group 2018. Oregon State University. <http://prism.oregonstate.edu> (accessed 9 September 2018).
- Radcliffe, D.E., Šimůnek, J., 2010. *Soil Physics with HYDRUS: Modeling and Applications.* CRC Press, Boca Raton, FL.
- Rawls, W.J., Brakensiek, D.L., Saxton, K.E., 1982. Estimation of Soil Water Properties. *Trans. ASAE.* <https://doi.org/10.13031/2013.33720>.
- Reynolds, W.D., Elrick, D.E., 1985. In situ measurement of field-saturated hydraulic conductivity, sorptivity, and the  $\alpha$ -parameter using the guelph permeameter. *Soil Sci.* <https://doi.org/10.1097/00010694-198510000-00008>.
- Richards, L.A., 1931. Capillary conduction of liquids through porous mediums. *J. Appl. Phys.* doi 10 (1063/1), 1745010.
- Schaap, M.G., Leij, F.J., Van Genuchten, M.T., 2001. Rosetta: A computer program for estimating soil hydraulic parameters with hierarchical pedotransfer functions. *J. Hydrol.* [https://doi.org/10.1016/S0022-1694\(01\)00466-8](https://doi.org/10.1016/S0022-1694(01)00466-8).
- Schietecatte, W., Ouessar, M., Gabriels, D., Tanghe, S., Heirman, S., Abdelli, F., 2005. Impact of water harvesting techniques on soil and water conservation: a case study on a micro catchment in southeastern Tunisia. *J. Arid Environ.* <https://doi.org/10.1016/j.jaridenv.2004.09.022>.
- Selker, J.S., Assouline, S., 2017. An explicit, parsimonious, and accurate estimate for ponded infiltration into soils using the green and ampt approach. *Water Resour. Res.* <https://doi.org/10.1002/2017WR021020>.
- Selker, J.S., Keller, K., McCord, J., 1999. *Vadose zone processes.* CRC Press, Boca Raton, Fla, pp. 339.
- Šimůnek, J., Bradford, S.A., 2008. Vadose zone modeling: introduction and importance. *Vadose Zo. J.* <https://doi.org/10.2136/vzj2008.0012>.
- Šimůnek, J., van Genuchten, M.T., 2008. Modeling nonequilibrium flow and transport processes using HYDRUS. *Vadose Zo. J.* <https://doi.org/10.2136/vzj2007.0074>.
- Šimůnek, J., van Genuchten, M.T., Sejna, M., 2012. HYDRUS: Model use, calibration, and validation. *Trans. Am. Soc. Agric. Biol. Eng.* <https://doi.org/10.1029/2002WR001340>.
- Siyal, A.A., Bristow, K.L., Šimůnek, J., 2012. Minimizing nitrogen leaching from furrow irrigation through novel fertilizer placement and soil surface management strategies. *Agric. Water Manag.* <https://doi.org/10.1016/j.agwat.2012.09.008>.
- Sukhija, B.S., Reddy, D.V., Nagabhushanam, P., Hussain, S., 2003. Recharge processes: piston flow vs preferential flow in semi-arid aquifers of India. *Hydrogeol. J.* <https://doi.org/10.1007/s10040-002-0243-3>.
- van Genuchten, M.T., 1980. Closed-form equation for predicting the hydraulic conductivity of unsaturated soils. *Soil Sci. Soc. Am. J.* <https://doi.org/10.2136/sssaj1980.03615995004400050002x>.
- Wang, J., Huang, G., Zhan, H., Mohanty, B.P., Zheng, J., Huang, Q., Xu, X., 2014. Evaluation of soil water dynamics and crop yield under furrow irrigation with a two-dimensional flow and crop growth coupled model. *Agric. Water Manag.* <https://doi.org/10.1016/j.agwat.2014.04.007>.
- Wang, W., Neuman, S.P., Yao, T.M., Wierenga, P.J., 2003. Simulation of large-scale field infiltration experiments using a hierarchy of models based on public, generic, and site data. *Vadose Zo. J.* <https://doi.org/10.2113/2.3.297>.
- Wösten, J.H.M., Pachepsky, Y.A., Rawls, W.J., 2001. Pedotransfer functions: Bridging the gap between available basic soil data and missing soil hydraulic characteristics. *J. Hydrol.* [https://doi.org/10.1016/S0022-1694\(01\)00464-4](https://doi.org/10.1016/S0022-1694(01)00464-4).
- Xu, C., Zhang, H., Huang, J., Zhang, Y., Wu, J., Schaap, M.G., Zeng, W., 2017. Inversion of root zone soil hydraulic parameters with limited calibration data. *Soil Sci. Soc. Am. J.* <https://doi.org/10.2136/sssaj2016.09.0308>.
- Zhang, Zhuanfang F., Groenevelt, Pieter H., Parkin, Gary W., 1998. The well-shape factor for the measurement of soil hydraulic properties using the Guelph Permeameter. *Soil Tillage Res.* 49 (3), 219–221. [https://doi.org/10.1016/S0167-1987\(98\)00174-3](https://doi.org/10.1016/S0167-1987(98)00174-3).
- Zhang, Y., Schaap, M.G., Guadagnini, A., Neuman, S.P., 2016. Inverse modeling of unsaturated flow using clusters of soil texture and pedotransfer functions. *Water Resour. Res.* <https://doi.org/10.1002/2016WR019016>.
- Ziadat, F., Mazahreh, S., Haddad, M., Benabdellouahab, T., Kandakji, T., Attaher, S., Oweis, T.Y., Karrou, M., 2014. Similarity and Suitability Analysis to Assist the Out-Scaling of Sustainable Water and Land Management Practices in West Asia and North Africa. Lebanon.
- Zobeck, T.M., Fausey, N.R., Hamdan, N.S., 1985. Effect of sample cross-sectional area on saturated hydraulic conductivity in two structured clay soils. *Trans. ASAE.*